

## Circulenes

Deutsche Ausgabe: DOI: 10.1002/ange.201913552  
Internationale Ausgabe: DOI: 10.1002/anie.201913552**Anti-Aromatic versus Induced Paratropicity: Synthesis and Interrogation of a Dihydro-diazatrioxa[9]circulene with a Proton Placed Directly above the Central Ring**

Stephan K. Pedersen, Kristina Eriksen, Nataliya N. Karaush-Karmazin, Boris Minaev, Hans Ågren, Gleb V. Baryshnikov\* und Michael Pittelkow\*

**Abstract:** We present a high-yielding intramolecular oxidative coupling within a diazadioxa[10]helicene to give a dihydro-diazatrioxa[9]circulene. This is the first [n]circulene containing more than eight ortho-annulated rings ( $n > 8$ ). The single-crystal X-ray structure reveals a tight columnar packing, with a proton from a pendant naphthalene moiety centred directly above the central nine-membered ring. This distinct environment induces a significant magnetic deshielding effect on that particular proton as determined by  $^1\text{H}$  NMR spectroscopy. The origin of the deshielding effect was investigated computationally in terms of the NICS values. It is established that the deshielding effect originates from an induced paratropic ring current from the seven aromatic rings of the [9]circulene structure, and is not due to the nine-membered ring being antiaromatic. UV/Vis spectroscopy reveals more efficient conjugation in the prepared diazatrioxa[9]circulene compared to the parent helical azaoxa[10]helicenes, and DFT calculations, including energy levels, confirm the experimental observations.

**Introduction**

Aromaticity and anti-aromaticity are phenomena that have received significant attention both from experimental and from theoretical chemists over the years.<sup>[1–3]</sup> The famous Hückel  $4n + 2$  rule describes aromatic compounds such as

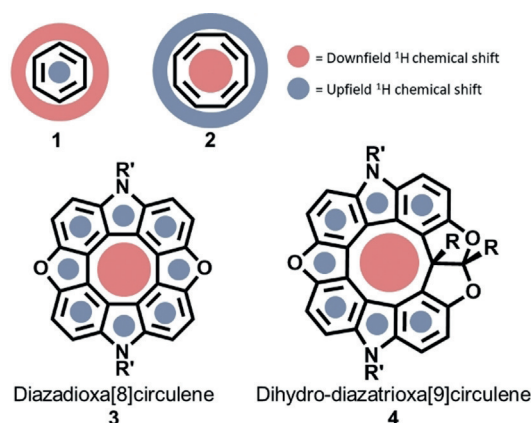


**Figure 1.** Simplified illustration of the influence of diatropic and paratropic ring currents on the  $^1\text{H}$  chemical shift inside and outside of select aromatic, anti-aromatic, and non-aromatic rings.

benzene (**1**) while the  $4n$  rule describes anti-aromatic systems such as planarized cyclooctatetraene (**2**; Figure 1).<sup>[4]</sup> Generally speaking, aromatic compounds are chemically stable, while anti-aromatic compounds are unstable. Studies of planar, thus anti-aromatic, cyclooctatetraene (**2**) are only possible in the realm of computational chemistry.<sup>[5]</sup> In recent years, several examples of chemically stable anti-aromatic molecules have been described, including a range of planar cyclooctatetraenes imbedded in [8]circulene structures (**3**), nor-corrole structures, and indeno[1,2-*b*]fluorene structures.<sup>[6–10]</sup> A prevalent strategy to stabilize anti-aromatic rings, within a molecule, is to anneal the anti-aromatic segment with aromatic rings.<sup>[3,11]</sup> This is the case for diazadioxa[8]circulene **3**, where the eight aromatic rings form a planar cyclooctatetraene motif (Figure 1).<sup>[8]</sup> From a computational perspective, a convenient determination of aromaticity is a negative nuclear independent chemical shift (NICS) value due to the diatropic ring current, while anti-aromatic rings have positive NICS values as a consequence of a paratropic ring current.<sup>[12,13]</sup> The influence of these ring currents on  $^1\text{H}$  chemical shifts is illustrated for **1** and **2** in Figure 1. The NICS predictions for molecule **3** are difficult to test experimentally, by  $^1\text{H}$  NMR spectroscopy, as it requires the preparation of compounds with a proton placed directly above the aromatic or anti-aromatic ring under investigation.<sup>[14]</sup> The obtained NICS values are convoluted by the influence of the aromatic ring(s) used to anneal and stabilize the central postulated anti-aromatic ring that they form.<sup>[15–17]</sup>

[\*] Dr. S. K. Pedersen, K. Eriksen, Prof. M. Pittelkow  
University of Copenhagen  
Department of Chemistry  
Universitetsparken 5, 2100 Copenhagen Ø (Denmark)  
E-Mail: pittel@chem.ku.dk

Dr. N. N. Karaush-Karmazin, Prof. B. Minaev  
Department of Chemistry and Nanomaterials Science  
Bohdan Khmelnytsky National University  
18031 Cherkasy (Ukraine)

Prof. H. Ågren, Prof. G. V. Baryshnikov  
Division of Theoretical Chemistry and Biology  
School of Engineering Sciences in Chemistry, Biotechnology and  
Health, KTH Royal Institute of Technology  
10691 Stockholm (Sweden)  
E-Mail: glibar@kth.se

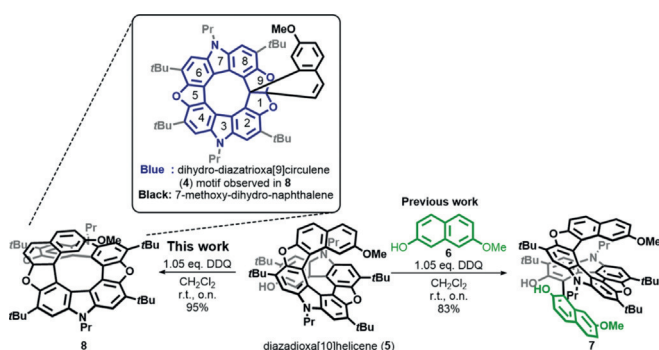
Prof. H. Ågren  
College of Chemistry and Chemical Engineering  
Henan University, Kaifeng, Henan 475004 (P. R. China)

Supporting information and the ORCID identification number(s) for the author(s) of this article can be found under:  
<https://doi.org/10.1002/anie.201913552>.

In a specific case, such as diazadioxo[8]circulene (**3**) and related hetero[8]circulenes, the central eight-membered ring has experimentally been determined to have positive NICS values.<sup>[8,12,18]</sup> This can either be due to the presence of the paratropic ring current of an anti-aromatic COT motif, or be due to the influence of the diatropic ring currents of the surrounding aromatic rings, that is, induced paratropicity. Herein, we describe a scenario where this exact problem is addressed, both experimentally and computationally. We report on the synthesis of a dihydro[9]circulene derivative (**4**), where the central non-aromatic nine-membered ring fulfils two of the criteria for anti-aromaticity: positive calculated NICS values and a downfield shift of the resonance of a proton positioned above the centre of the ring. The dihydro[9]circulene derivative is prepared by a high-yielding intramolecular oxidative coupling within a diazadioxo[10]helicene. The single-crystal X-ray structure reveals a tight columnar packing, with the *peri*-proton from a naphthalene moiety centred directly above the central nine-membered ring. This distinct chemical environment induces a significant downfield shift on the resonance of said proton as determined by <sup>1</sup>H NMR spectroscopy, which is consistent with the positive NICS values determined computationally. As the central nine-membered ring of the dihydro[9]circulene is unambiguously non-aromatic, the deshielding effect is due to the diatropic ring current of surrounding aromatic rings in the dihydro[9]circulene structure, and not due to the central nine-membered ring being antiaromatic.

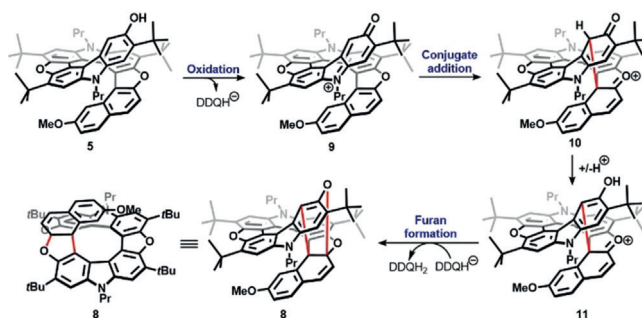
## Results and Discussion

Previously we have reported on the DDQ-mediated oxidative hetero-coupling between diazadioxo[10]helicene **5** and 7-methoxy-2-naphthol (**6**) giving **7** (Scheme 1).<sup>[19]</sup> In this work it is presented how, by conducting the reaction without naphthol **6**, we access the intramolecular oxidative coupling product **8** in very high yield. Compound **8** contains a 7-methoxy-dihydronaphthalene orthogonally positioned above a [9]circulene (**4**) system (highlighted in blue for structure **8**, see the box in Scheme 1). Peculiar reactivity within the aromatic skeleton of helicenes has also been



**Scheme 1.** Previously reported synthesis of [10]helicene **7** and the herein reported synthesis of **8**, containing [9]circulene motif **4**.

reported by the groups of Fuchter and Katz for the intramolecular rearrangement of carba[7]helicene and derivatives thereof, forming the carba[6]circulene motifs.<sup>[20–22]</sup> It should be noted that thus far the biggest carba- and hetero-[*n*]circulenes reported are *n* = 8, and the properties and structures of higher-order [*n*]circulenes have only been investigated theoretically.<sup>[6,23–25]</sup> The dihydro[9]circulene is the first [*n*]circulene motif with *n* > 8. Formally, the motif is a dihydro-diazatrioxa[9]circulene as illustrated in **4**, with rings 2–8 being fully aromatic, and dihydrofuran rings 1 and 9 being annulated via two sp<sup>3</sup> carbon atoms. Our mechanistic proposal for the formation of **8**, from **5** by treatment with DDQ, is presented in Scheme 2. Initial oxidation, mediated



**Scheme 2.** Mechanistic proposal for the formation **8**. Bonds formed during the reaction are shown in red.

by DDQ, on the hydroxy termini of **5** forms the quinoidal species **9**. Alternatively, a one-electron mechanism could also be a plausible pathway.<sup>[26,27]</sup> Conjugate addition from the 2-position of the furan positioned directly beneath the furan ring within the helicene framework gives oxocarbenium intermediate **10**, which tautomerizes to phenol **11**. It should be noted that in the crystal structure of **10**, the carbon atoms between which the bond is formed are placed directly above each other and are only 3.26 Å apart. The nucleophilic phenol termini of **11** can then undergo intramolecular furan formation, which upon deprotonation, likely by the monoanionic hydroquinone of DDQ, forms the [9]circulene **8**.

The structure of **8** was unambiguously determined by single crystal X-ray diffraction (SCXRD), with the crystals readily obtained by slow evaporation from a mixture of CH<sub>2</sub>Cl<sub>2</sub> and EtOH. Focusing on **8**, it is observed that the two sp<sup>3</sup> carbon atoms protrude the plane formed by the aromatic segment of the [9]circulene motif (Figure 2a). The central nine-membered ring has a diameter of about 4 Å. Looking top down on **8**, the naphthalene is positioned at a slight angle relative to the symmetry axis of the [9]circulene (Figure 2b). As a result, **8** is chiral in the solid state, with the enantiomers consisting of the naphthalene motif tilted either to the left (as seen in Figure 2b) or to the right. The unit cell consists of both enantiomers, forming an overall achiral structure in the solid state (Figure 2c). Looking at the overall packing of **8**, it forms columns consisting of alternating unit cells (Figure 2d). From the solid-state structure, it is observed that the naphthalene is positioned in such a manner that the *peri*-proton of the naphthalene (H<sub>a</sub>, highlighted in green, Figure 2a), is posi-

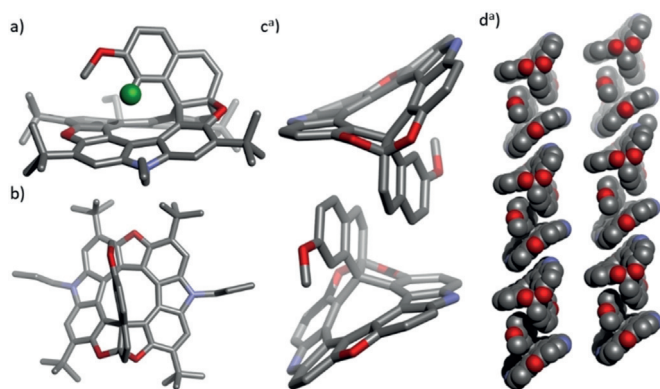


**Figure 2.** a, b) Crystal structure, c) unit cell, and d) packing of **8** observed in the solid state.  $H_a$  is highlighted in green. [a] The *tert*-butyl and *n*-propyl side chains have been removed for clarity.<sup>[B5]</sup>

tioned almost directly above the centre of the [9]circulene ring. The distances from the highlighted proton ( $H_a$ ) to the nearest  $sp^2$  carbon atoms of the nine-membered ring range from 3.48(2) Å to 2.42(7) Å, and the distance from the plane formed by the inner  $sp^2$  carbon atoms of the nine-membered ring is approximately 1.9 Å in the solid state.

The positioning of the *peri*-proton ( $H_a$ ) above the centre of the dihydro[9]circulene ring has a pronounced influence on its chemical shift, as determined by  $^1H$  NMR spectroscopy (Figure 3). For the diazadioxo[10]helicene **5**, the resonance of  $H_a$  is located at 7.16 ppm, whereas for **8**, it is situated at

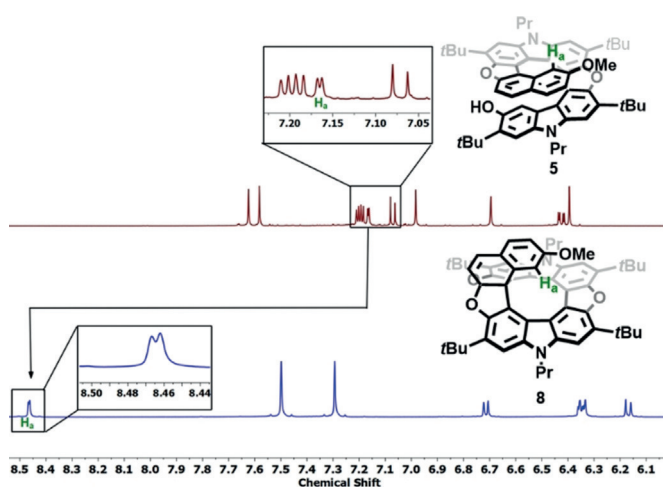


**Figure 3.** Aromatic regions of the  $^1H$  NMR spectra of diazadioxo[10]helicene **5** and dihydro-diazatrioxo[9]circulene **8** recorded in  $CD_2Cl_2$ . See the Supporting Information, Figure S1 for the full spectra.

8.46 ppm, which amounts to a total downfield shift of 1.30 ppm when comparing the two substrates. For comparison, the chemical shifts of the corresponding protons in 2,7-dimethoxynaphthalene and anisole are 7.08 ppm and 6.90 ppm in  $CD_2Cl_2$ , respectively (see the Supporting Information, Figures S2 and S3 for  $^1H$  NMR spectra). Both values are comparable to the chemical shift observed in helicene **5**,

indicating that the surrounding helical environment has little influence on the chemical shift of  $H_a$ .

To further understand the electronic factors that influence the drastic deshielding effect on  $H_a$ , we conducted NICS calculations for each local ring of [9]circulene **8** and [10]helicene **5** (along the inner main (long) axis of the latter; Figure 4). It is clear from the calculations that the slightly twisted  $C_9$  inner ring of dihydro[9]circulene **8** possesses a significant paratropic contribution in a quite narrow region (1 Å up, 1 Å down and 0.75 Å to the left/right from the centre point of the  $C_9$  ring). Conveniently, the  $H_a$  proton is situated in this narrow paratropic region, which can explain the downfield shift of 1.3 ppm observed by  $^1H$  NMR spectroscopy. Our calculations of the isotropic shielding tensor for proton  $H_a$  in the diazadioxo[10]helicene **5** and dihydro[9]circulene **8** provide a downfield shift of 1.0 ppm, which is in good agreement with the result obtained experimentally. The paratropic magnetically induced ring currents inside the  $C_9$  ring are likely due to the strong global diatropic ring currents of the condensed five- and six-membered rings (rings 2–8 in **4**, Scheme 1). Indeed, NICS(0)/(1) values for each condensed pyrrole, furan, and benzene ring indicate their expected aromatic character. The  $H_a$ -containing benzene ring is also predicted to be typically aromatic and that is why a negative NICS value is observed in regions proximal to this ring (NICS(1.5) in Figure 4a). Looking below the plane of **5**, NICS(–2) values are also negative, which can be explained in terms of the long-ranging diatropic contribution from the adjacent aromatic rings, which are twisted relative to the central axis. In fact, herein, we have presented the first experimental and theoretical evidence for the existence of strong paratropic ring currents in closed-circle heterocirculenes, by making use of a covalently linked system. Moving to the diazadioxo[10]helicene **5**, it also possesses strong paratropic currents inside the helix as follows from the positive NICS values calculated along the main axis of the inner helix. These values reach a maximum of 5.0 ppm, which is comparable to the highest value observed in **8** (5.61 ppm). This fact again confirms that the anticlockwise-circulating paratropic currents inside the helix are topologically induced, that is, they are caused by the strong clockwise global diatropic currents. Such a phenomenon was recently discussed.<sup>[28]</sup>

To further clarify the electronic properties of **5** and **8**, our attention was turned to TD-DFT calculations. The optimized structure of dihydro[9]circulene **8** in the ground electronic state is conformationally and geometrically the same as the one obtained by the SCXRD data. The calculated conformation of diazadioxo[10]helicene **5** in the  $S_0$  state expectedly looks like a right-handed helix (the left-handed enantiomer is energetically identical). The distance between the helix edges is approximately 3.6 Å. Upon excitation to the  $S_1$  state of the [10]helicene (**5**), the distance between the helix edges becomes 0.15 Å larger indicating considerable flexibility of the [10]helicene, whereas for excitation of dihydro[9]circulene **8** into the  $S_1$  or  $T_1$  state, the molecular conformation and structural parameters are not changed significantly. As follows from the calculated vertical absorption spectra, the  $S_1$  and  $T_1$  states for each studied molecule (**5** and **8**) are of the same electronic configuration and correspond to

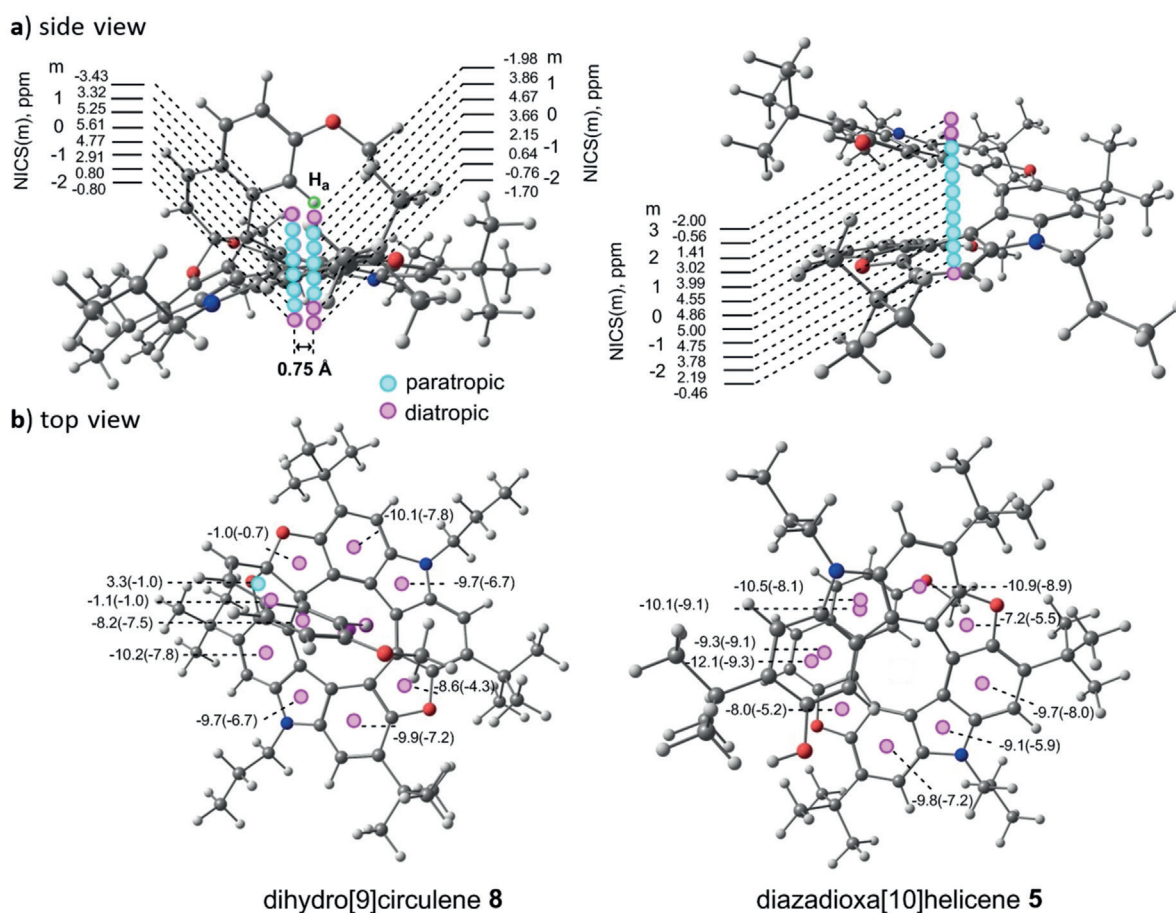


**Figure 4.** a) Side and b) top views showing the NICS(m) values for diazadioxa[10]helicene **5** and dihydro[9]circulene **8**. For the top-view figures, the numbers correspond to the NICS(0)/NICS(1) calculations.

the HOMO–LUMO excitations. As can be seen from Figure 5, the HOMO and LUMO wavefunctions for the dihydro[9]circulene **8** correspond to  $\pi$ -type orbitals that are similar to those of the related hetero[8]circulenes in terms of their bonding/antibonding character. The HOMO and LUMO wavefunctions for diazadioxa[8]circulene **3** are presented for comparison in Figure 5.<sup>[8,29,30]</sup> It is even possible to observe a similarity between the HOMO and LUMO patterns of the open-circle diazadioxa[10]helicene **5** and closed-circle dihydro[9]circulene **8**. The electronic properties of the dihydro[9]circulene (**8**) were studied by UV/Vis and fluorescence spectroscopy in  $\text{CH}_2\text{Cl}_2$  and compared to those of the parent diazadioxa[10]helicene (**5**; Figure 6). The vibronic progression observed in **5** is maintained in **8**, with the most prominent feature being the strongest electronic transition ( $\lambda_{\text{max}}$ ) in the visible spectrum located at almost the same wavelength ( $\lambda_{\text{max}} = 350$  nm for **8** and  $\lambda_{\text{max}} = 353$  nm for **5**). Looking at the longest-wavelength absorption maxima ( $\lambda_{0-0}$ ) a bathochromic shift of 7 nm was observed for **8** relative to **5** ( $\lambda_{0-0} = 428$  nm for **8**,  $\lambda_{0-0} = 421$  nm for **5**). This is an interesting feature as the diazadioxa[10]helicene **5** contains a total of ten annulated aromatic groups, whereas dihydro-diazadioxa[9]circulene **8** only contains seven annulated aromatic rings (rings 2–8 as shown for **4** in Scheme 1), which should result in a lower HOMO–LUMO gap for **8**.<sup>[31,32]</sup> This indicates a more

efficient  $\pi$ -conjugation in the planar aromatic segment of dihydro[9]circulene **8** compared to the helical aromatic skeleton of [10]helicene **5**. Diazadioxa[3]circulene **3** has a very similar lowest-energy absorption (425 nm). Comparing the emissive properties of dihydro[9]circulene **8** ( $\lambda_{\text{em}} = 448$  nm) and [10]helicene **5** ( $\lambda_{\text{em}} = 457$  nm), **5** has an appreciably larger Stokes shift than the dihydro[9]circulene **8**,  $1870$   $\text{cm}^{-1}$  vs.  $1040$   $\text{cm}^{-1}$ , respectively. The fluorescence quantum yield of **8** ( $\Phi_{\text{fl}} = 0.13$ ) is less than half of the measured value of **5** ( $\Phi_{\text{fl}} = 0.27$ ). Despite a similarity in the shapes and energies of the frontier molecular orbitals for compounds **8** and **5**, the transitions responsible for their spectral properties are considerably different. As can be seen from Table 1, the first singlet–singlet electronic transition ( $S_0$ – $S_1$ ) for the diazadioxa[10]helicene **5** is 2.5 times less intensive than the second one ( $S_0$ – $S_2$ ). The opposite situation is observed for the dihydro[9]circulene **8**: the  $S_0$ – $S_1$  transition is 4.2 times more intensive than the next  $S_0$ – $S_2$  transition. The energy differences between the  $S_1$  and  $S_2$  excited states (in vertical approximation) for both compounds are 27 nm. We experimentally observed the first band at 421 nm for diazadioxa[10]helicene **5**, which is mainly affected by the  $S_0$ – $S_2$  transition, and at 428 nm for dihydro[9]circulene **8** corresponding predominantly to the  $S_0$ – $S_1$  transition. The next experimentally observed band at around 400 nm can be assigned to the

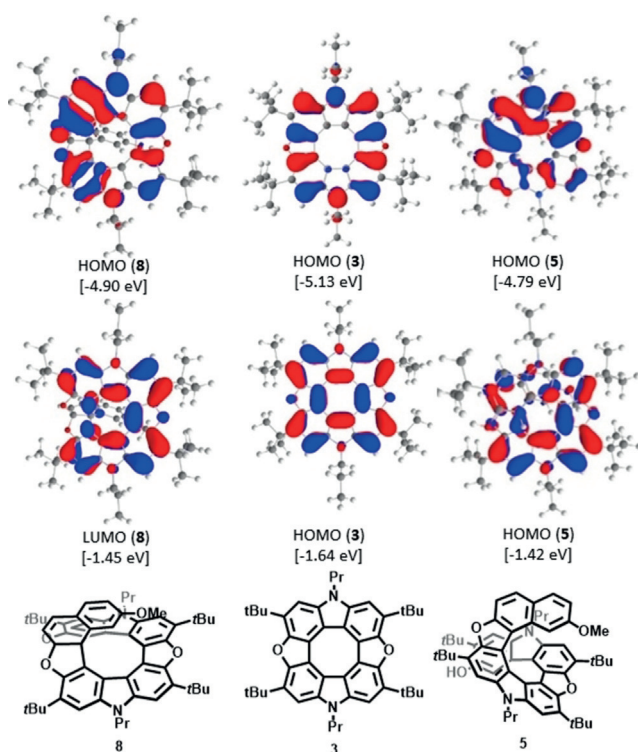


**Figure 5.** Frontier molecular orbitals for diazadioxo[10]helicene **5** and dihydro[9]circulene **8** calculated by the (PCM)/B3LYP/6-31G(d) method and those for diazadioxo[8]circulene **3** as a reference, calculated by the same method.

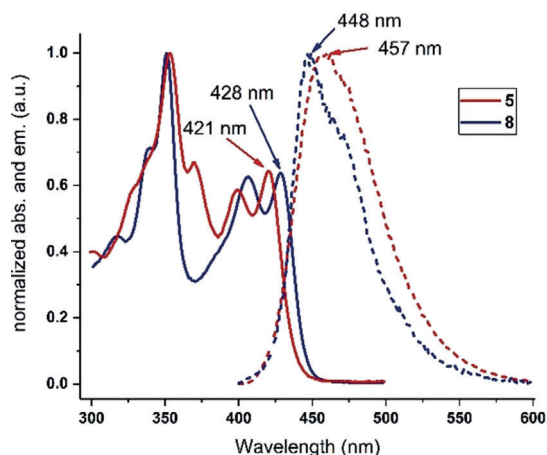


**Figure 6.** Normalized absorption and emission spectra of **8** and **5**, recorded in  $\text{CH}_2\text{Cl}_2$ .

vibronic satellite of the first (main) band and particularly of the  $S_0$ – $S_1$  transition for dihydro[9]circulene **8** and the  $S_0$ – $S_2$  transition for diazadioxo[10]helicene **5**. As the fluorescence originates from the  $S_1$  excited state by radiative relaxation, we have predicted a red-shift of 18 nm for the fluorescence of diazadioxo[10]helicene (**5**) with respect to the fluorescence maximum of dihydro[9]circulene (**8**). This is in good agreement with the experimentally observed value of 9 nm. The vibronic progression of the  $S_1$ – $S_0$  transition is also observed in the experimental emission spectrum (at ca. 457 nm for **8**).

**Tabelle 1:** The energies and intensities of the low-lying singlet–singlet electronic transitions for the ground state (vertical absorption) and  $S_1$  excited state (vertical emission) geometries at the (PCM)/B3LYP/6-31G(d) level of theory.

Property	<b>5</b>	<b>8</b>
$\lambda_{\text{abs}}^{\text{vert}}(S_1)$ [nm]	436	420
$f_{\text{abs}}^{\text{vert}}(S_0 \rightarrow S_1)$	0.081	0.256
[exp.]	[-]	[428 ( $S_1 + S_2$ )]
$\lambda_{\text{abs}}^{\text{vert}}(S_2)$ [nm]	409	393
$f_{\text{abs}}^{\text{vert}}(S_0 \rightarrow S_2)$	0.203	0.061
[exp.]	[421 ( $S_1 + S_2$ )]	[-]
$\lambda_{\text{em}}^{\text{vert}}(S_1)$ [nm]	485	467
$f_{\text{em}}^{\text{vert}}(S_1 \rightarrow S_0)$	0.187	0.425
[exp.]	[457]	[448]

From Table 1 the intensity of the vertical  $S_1$ – $S_0$  transition calculated by taking into account the geometry relaxation in the  $S_1$  state increases by more than a factor of two relative to the same transition calculated at the  $S_0$  state geometry (for both compounds **5** and **8**). Surprisingly, despite the twice higher intensity of the  $S_1$ – $S_0$  transition for dihydro[9]circulene **8** ( $\Phi_{\text{fl}} = 0.13$ ) relative to [10]helicene **5** ( $\Phi_{\text{fl}} = 0.27$ ) it demonstrates half the fluorescence quantum yield. This feature can be explained in terms of a much stronger spin–orbit coupling (SOC) between the  $S_1$  and  $T_1/T_2$  states for dihydro[9]circulene **8**, which promotes the quenching of  $S_1$  fluorescence by the fast  $S_1$ – $T_1$  and  $S_1$ – $T_2$  intersystem crossing pathways (Figure 7).

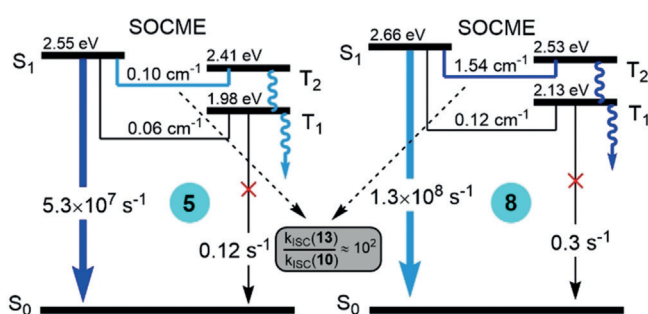


**Figure 7.** The mechanism of  $S_1$  state deactivation for diazadioxo[10]helicene **5** and dihydro[9]circulene **8** in accordance with the (COSMO)/B3LYP/DZP calculations taking spin–orbit coupling effects into account.

Taking into account that the  $S_1$ – $T_2$  energy gap is almost the same (about 0.13 eV) for compounds **5** and **8**, the reorganization energies upon the  $S_1$ – $T_2$  non-radiative transition are close to the same value for both compounds. Thus, the rate constant ( $k_{\text{ISC}}$ ) for the  $S_1$ – $T_2$  ISC should be only proportional to the corresponding squared spin–orbit coupling element (SOCME), that is, to the  $\langle S_1 | \hat{H}_{\text{SO}} | T_2 \rangle^2$  value (in the framework of the Fermi golden rule and Marcus–Levich–Jortner theory).<sup>[33,34]</sup> As follows from our calculations, the  $\langle S_1 | \hat{H}_{\text{SO}} | T_2 \rangle$  SOCME for circulene **8** amounts to  $1.54 \text{ cm}^{-1}$  vs. only  $0.1 \text{ cm}^{-1}$  for helicene **5**, which means that the  $k_{\text{ISC}}$  value is at least two orders of magnitude larger for compound **8** (without accounting for  $S_1$ – $T_1$  quenching because of the

comparatively large  $S_1$ - $T_1$  energy gap). This fact explains the less efficient fluorescence of circulene **8** despite the higher rate constant of the fluorescence process.

## Conclusion

In summary, we have synthesized previously unknown [9]circulene **8**, formally a dihydro-diazatrioxa[9]circulene. This motif was formed by a high-yielding intramolecular oxidative coupling of hydroxy-terminated diazadioxa[10]helicene **5**. The structure of [9]circulene **8** was unambiguously determined by X-ray crystallography. A proton is positioned directly above the nine-membered ring of the [9]circulene motif. This unique chemical environment has a pronounced deshielding effect on the proton, as determined by  $^1\text{H}$  NMR spectroscopy. Compared to the parent diazadioxa[10]helicene **5**, the proton is shifted downfield by a remarkable 1.30 ppm in the [9]circulene (**8**). Nucleus-independent chemical shift (NICS) calculations indicate that the deshielding effect can be attributed to an induced paramagnetic environment. These results can serve as reference points for researchers investigating the phenomena of anti-aromaticity by NICS calculations and/or NMR experiments. Ongoing studies concern the synthesis of the fully aromatic diazatrioxa[9]circulene motif and higher-order azaoxa[ $n$ ]circulenes.

## Acknowledgements

G.V.B. and H.Å. thank the Olle Engkvist Byggmästare foundation for support (189-0223). G.V.B. and B.M. are thankful for support from the Ministry of Education and Science of Ukraine (0117U003908 and 0118U003862). The calculations were performed with computational resources provided by the High Performance Computing Center North (HPC2N) in Umeå, Sweden through the project „Multi-physics Modeling of Molecular Materials“ SNIC 2018-2-38. We acknowledge support from the Danish Council for Independent Research (DFR 4181-00206 and 9040-00265) and from the University of Copenhagen.

## Conflict of interest

The authors declare no conflict of interest.

**Stichwörter:** Antiaromatizität · Circulene · Kondensierte Ringe · Neungliedrige Ringe · NICS-Werte

**Zitierweise:** *Angew. Chem. Int. Ed.* **2020**, *59*, 5144–5150  
*Angew. Chem.* **2020**, *132*, 5182–5188

- 
- [1] R. Breslow, *Acc. Chem. Res.* **1973**, *6*, 393–398.  
[2] Z. Zeng, X. Shi, C. Chi, J. T. López Navarrete, J. Casado, J. Wu, *Chem. Soc. Rev.* **2015**, *44*, 6578–6596.  
[3] R. Breslow, *Chem. Rec.* **2014**, *14*, 1174–1182.

- [4] E. Hückel, *Z. Phys.* **1931**, *70*, 204–286.  
[5] T. Nishinaga, T. Ohmae, M. Iyoda, *Symmetry* **2010**, *2*, 76–97.  
[6] a) T. Hensel, N. N. Andersen, M. Plesner, M. Pittelkow, *Synlett* **2015**, 27, 498–525; b) S. Kato, Y. Serizawa, D. Sakamaki, S. Seki, Y. Miyake, H. Shinokubo, *Chem. Commun.* **2015**, *51*, 16944–16945; c) X. Xiong, C.-L. Deng, B. F. Minaev, G. V. Baryshnikov, X.-S. Peng, H. N. C. Wong, *Chem. Asian J.* **2015**, *10*, 969–975; d) F. Chen, Y. S. Hong, D. Kim, T. Tanaka, A. Osuka, *Chem-PlusChem* **2017**, *82*, 1048–1051.  
[7] J. H. Dopfer, H. Wynberg, *J. Org. Chem.* **1975**, *40*, 1957–1966.  
[8] T. Hensel, D. Trpceviski, C. Lind, R. Grosjean, P. Hammershøj, C. B. Nielsen, T. Brock-Nannestad, B. E. Nielsen, M. Schau-Magnussen, B. Minaev, G. V. Baryshnikov, M. Pittelkow, *Chem. Eur. J.* **2013**, *19*, 17097–17102.  
[9] D. T. Chase, B. D. Rose, S. P. McClintock, L. N. Zakharov, M. M. Haley, *Angew. Chem. Int. Ed.* **2011**, *50*, 1127–1130; *Angew. Chem.* **2011**, *123*, 1159–1162.  
[10] a) T. Ito, Y. Hayashi, S. Shimizu, J. Y. Shin, N. Kobayashi, H. Shinokubo, *Angew. Chem. Int. Ed.* **2012**, *51*, 8542–8545; *Angew. Chem.* **2012**, *124*, 8670–8673; b) M. Yamashina, Y. Tanaka, R. Lavendomme, T. Ronson, M. Pittelkow, J. R. Nitschke, *Nature* **2019**, *574*, 511–514.  
[11] X. Y. Wang et al., *Nat. Commun.* **2017**, *8*, 1948.  
[12] G. V. Baryshnikov, B. F. Minaev, M. Pittelkow, C. B. Nielsen, R. Salcedo, *J. Mol. Model.* **2013**, *19*, 847–850.  
[13] Z. Chen, C. S. Wannere, C. Corminboeuf, R. Puchta, P. v. R. Schleyer, *Chem. Rev.* **2005**, *105*, 3842–3888.  
[14] Y. Nakamura, N. Aratani, A. Osuka, *Chem. Asian J.* **2007**, *2*, 860–866.  
[15] K. Uehara, P. Mei, T. Murayama, F. Tani, H. Hayashi, M. Suzuki, N. Aratani, H. Yamada, *Eur. J. Org. Chem.* **2018**, 4508–4511.  
[16] K. Uehara, P. Mei, T. Murayama, F. Tani, H. Hayashi, M. Suzuki, N. Aratani, H. Yamada, *Eur. J. Org. Chem.* **2019**, 860–861.  
[17] A. Stanger, *Eur. J. Org. Chem.* **2019**, 857–859.  
[18] F. Chen, Y. S. Hong, S. Shimizu, D. Kim, T. Tanaka, A. Osuka, *Angew. Chem. Int. Ed.* **2015**, *54*, 10639–10642; *Angew. Chem.* **2015**, *127*, 10785–10788.  
[19] S. K. Pedersen, K. Eriksen, M. Pittelkow, *Angew. Chem. Int. Ed.* **2019**, *58*, 18419–18423; *Angew. Chem.* **2019**, *131*, 18590–18594.  
[20] M. J. Fuchter, M. Weimar, X. Yang, D. K. Judge, A. J. P. White, *Tetrahedron Lett.* **2012**, *53*, 1108–1111.  
[21] R. J. F. Berger, M. J. Fuchter, I. Krossing, H. S. Rzepa, J. Schaefer, H. Scherer, *Chem. Commun.* **2014**, *50*, 5251–5253.  
[22] D. Z. Wang, T. J. Katz, J. Golen, A. L. Rheingold, *J. Org. Chem.* **2004**, *69*, 7769–7771.  
[23] K. Y. Chernichenko, V. V. Sumerin, R. V. Shpanchenko, E. S. Balenkova, V. G. Nenajdenko, *Angew. Chem. Int. Ed.* **2006**, *45*, 7367–7370; *Angew. Chem.* **2006**, *118*, 7527–7530.  
[24] B. Napolion, F. Hagelberg, M. J. Huang, J. D. Watts, T. M. Simeon, D. Vereen, W. L. Walters, Q. L. Williams, *J. Phys. Chem. A* **2011**, *115*, 8682–8690.  
[25] H. Christoph, J. Grunenberg, H. Hopf, I. Dix, P. G. Jones, M. Scholtissek, G. Maier, *Chem. Eur. J.* **2008**, *14*, 5604–5616.  
[26] L. Zhai, R. Shukla, S. H. Wadumethrige, R. Rathore, *J. Org. Chem.* **2010**, *75*, 4748–4760.  
[27] S. Mallick, S. Maddala, K. Kollimalayan, P. Venkatakrishnan, *J. Org. Chem.* **2019**, *84*, 73–93.  
[28] G. V. Baryshnikov, R. R. Valiev, V. N. Cherepanov, N. N. Karaush-Karmazin, V. A. Minaeva, B. F. Minaev, H. Ågren, *Phys. Chem. Chem. Phys.* **2019**, *21*, 9246–9254.  
[29] B. F. Minaev, G. V. Baryshnikov, V. A. Minaeva, *Comput. Theor. Chem.* **2011**, 972, 68–74.  
[30] G. V. Baryshnikov, R. R. Valiev, N. N. Karaush, V. A. Minaeva, A. N. Sinelnikov, S. K. Pedersen, M. Pittelkow, B. F. Minaev, H. Ågren, *Phys. Chem. Chem. Phys.* **2016**, *18*, 28040–28051.

- [31] K. Nakanishi, D. Fukatsu, K. Takaishi, T. Tsuji, K. Uenaka, K. Kuramochi, T. Kawabata, K. Tsubaki, *J. Am. Chem. Soc.* **2014**, *136*, 7101–7109.
- [32] G. Bidan, A. De Nicola, V. Enée, S. Guillerez, *Chem. Mater.* **1998**, *10*, 1052–1058.
- [33] P. K. Samanta, D. Kim, V. Coropceanu, J. L. Brédas, *J. Am. Chem. Soc.* **2017**, *139*, 4042–4051.
- [34] J.-L. Bredas, D. Beljonne, V. Coropceanu, J. Cornil, *Chem. Rev.* **2004**, *104*, 4971–5004.
- [35] CCDC 1957224 (8) contains the supplementary crystallographic data for this paper. These data are provided free of charge by The Cambridge Crystallographic Data Centre.

Manuskript erhalten: 23. Oktober 2019  
Veränderte Fassung erhalten: 10. Dezember 2019  
Akzeptierte Fassung online: 21. Januar 2020  
Endgültige Fassung online: 20. Februar 2020